Heating ^{197}Au Nuclei with 8 GeV/c Antiproton and π^- Beams

T. Lefort,[1] K. Kwiatkowski,[1,*] W.-c. Hsi,[1] L. Pienkowski,[2] L. Beaulieu,[1] B. Back,[3] H. Breuer,[4] S. Gushue,[5] R. G. Korteling,[6] R. Laforest,[7] E. Martin,[7] E. Ramakrishnan,[7] L. P. Remsberg,[5] D. Rowland,[7] A. Ruangma,[7] V. E. Viola,[1] E. Winchester,[7] and S. J. Yennello[7]

[1]*Department of Chemistry and IUCF, Indiana University, Bloomington, Indiana 47405*
[2]*Heavy Ion Laboratory, Warsaw University, 02 097 Warsaw, Poland*
[3]*Physics Division, Argonne National Laboratory, 9700 S. Cass Avenue, Argonne, Illinois 60439*
[4]*Department of Physics, University of Maryland, College Park, Maryland 20742*
[5]*Department of Chemistry, Brookhaven National Laboratory, Upton, New York 11973*
[6]*Department of Chemistry, Simon Fraser University, Burnaby, British Columbia, Canada V5A 1S6*
[7]*Department of Chemistry and Cyclotron Laboratory, Texas A&M University, College Station, Texas 77843*

(Received 3 March 1999)

Comparison of the heating effect produced by 8 GeV/c π^- and antiproton beams incident on ^{197}Au nuclei has been conducted with the Indiana silicon sphere 4π detector array. Event reconstruction indicates formation of thermal-like heavy residues with excitation energies up to 1.7 GeV. Enhanced energy deposition is observed for antiprotons relative to negative pions. For events with excitation energies that exceed 1000 MeV, there is a 50% increase in cross section for the antiproton beam relative to the π^- beam. The predominant decay mode at these high excitation energies is multifragmentation in which three or more $Z \geq 3$ fragments are emitted.

PACS numbers: 25.70.Pq, 25.43.+t, 25.80.Hp

Antiproton beams provide an attractive mechanism for studying the thermal component of the nuclear equation of state in that they have been predicted to enhance high excitation-energy (E^*) events significantly relative to other hadron projectiles [1,2]. This E^* enhancement derives from the reabsorption of some fraction of the annihilation pions ($\langle n_\pi \rangle \simeq 5$), which complements the internal heating created by π-N and N-N scattering and Δ resonance excitation [1–3]. After the rapid thermalization of such systems [2,4], the most highly excited targetlike residues are expected to disintegrate primarily via multifragmentation events, believed to be the signal for a nuclear liquid-gas phase transition [5–7]. A further advantage, common to all hadron beams, is that they create a single source of thermal-like heavy residues, and at the same time minimize the dynamical effects due to the compression/decompression cycle and angular momentum associated with heavy-ion reactions.

The objective of the present research was to determine experimentally whether antiproton beams produce higher excitation energies than other hadrons in collisions with heavy nuclei, and if so, to quantify the magnitude of the effect. Previous experiments at LEAR with stopped antiprotons [8] and 2.1 GeV/c antiprotons [9] incident on heavy nuclei did not show evidence for enhanced deposition of excitation energy. While the 2.1 GeV/c measurements reported E^* values up to about 900 MeV, the probability for multifragmentation was found to be negligible. This result is consistent with the expected threshold of 800–1000 MeV for multifragmentation of Au-like systems [5–7]. Thus, more energetic antiprotons appear to be required in order to pursue multifragmentation studies with antiproton ($\bar{p}$) beams. However, studies with proton, π^-, and ^{3}He beams have demonstrated that once the beam energy exceeds about 6 GeV, there is little increase in the probability for forming high-E^* residues, primarily due to decreased nucleon stopping at higher energies [10–12]. Hence, a $\bar{p}$ momentum of 6–8 GeV/c would appear to be optimum for observing maximum excitation-energy deposition.

Observation of increased excitation-energy deposition with $\bar{p}$ beams would thus identify the antiproton as the optimum projectile for investigation of the thermal component of the nuclear equation of state. Of current interest in this regard would be extending the nuclear heating (caloric) curve [13] for thermally excited matter to the upper limits accessible to experiment. The data of Pochodzalla *et al.* [13], obtained in Au + Au collisions, suggest that the onset of nuclear vaporization may occur as low as $E^*/A \sim 10$–12 MeV for thermal-like systems—near the upper limits observed with p, π^-, and ^{3}He beams [12,14], but potentially accessible with $\bar{p}$ beams.

In order to address these questions experiment E900 was performed with a tagged secondary beam of 8.0 GeV/c negative particles ($\pi^-, K^-, \bar{p}$) at the Brookhaven National Laboratory Alternating Gradient Synchrotron (AGS) accelerator. Light-charged particles (LCP = H and He isotopes) and intermediate-mass fragments (IMF: $3 \leq Z \lesssim 16$) were measured with the Indiana silicon sphere (ISiS) 4π detector array [15]. Beams of $\sim 4 \times 10^6$ particles/cycle (4.5 s cycle time and $\approx$2.2 s spill flattop) were incident on a 2×2 cm^2 self-supporting ^{197}Au target foil of thickness 2 mg/cm^2. To minimize reactions due to the beam halo, the target was suspended on two 50 μm tungsten wires. Beam particles were tagged with a time-of-flight (TOF) Čerenkov-counter

identification system. The time-of-flight system employed a 12-mm-thick Bicron 418 plastic scintillator as a start detector and a 5-mm-thick Bicron 418 scintillator 64 m downstream as a stop element. Timing resolution (σ) was ≈200 ps and provided clean separation of $\bar{p}$ and π^- projectiles (8:1 peak-to-valley ratio). This permitted simultaneous measurement of the $\bar{p}$ and π^- reactions under identical conditions. Beam composition was ≈98% π^-, 1% K^-, and 1% $\bar{p}$ at the target. A CO_2 Čerenkov counter operated at atmospheric pressure was used to identify and veto negative pions that overlapped with the $\bar{p}$ distribution in the time-of-flight spectrum. A segmented halo-veto scintillator array, described in [11], operated in anticoincidence with the TOF-Č-ISiS coincidence signals.

The ISiS array consists of 162 gas-ion-chamber/500 μm silicon/28 mm CsI detector telescopes that cover approximately 74% of 4π and polar angles from 14°–86.5° and 93.5°–166° [15]. Charged particles with energies $1 \leq E/A \leq 92$ MeV were Z identified up to $Z \simeq 16$. Isotope resolution was obtained for H, He, and Li ejectiles in the energy range $8 \leq E/A \leq 92$ MeV. Also, unidentified fast charged particles (or "gray particles," primarily protons) with energies from 92 to 300 MeV were measured. The minimum-bias ISiS hardware trigger required fast signals in three or more silicon detectors, but did not include gray particles. The final data set analyzed here contained 24 000 $\bar{p}$ and 2.4×10^6 π^- events in coincidence with one or more He ions or IMFs.

An important measure of energy dissipation in GeV hadron and ^{3}He-induced reactions is the multiplicity of charged particles observed in an event [10]. In Fig. 1 we compare the multiplicity distributions of all observed charged particles (N_c) and IMFs ($N_{\rm imf}$) for the 8 GeV/c $\bar{p}$ and π^- beams. The total number of events for each beam is normalized to a total probability of $\sum N_i = 1$. It is observed that the high multiplicity events are significantly enhanced for the $\bar{p}$ beam in both distributions. This enhancement becomes more apparent when the ratio of the probability for a given multiplicity for each beam $[P(\bar{p})/P(\pi^-)]$ is examined as a function of multiplicity, as shown in the lower part of Fig. 1. In particular, the ratio increases by nearly an order of magnitude beyond $N_c \approx 20$. The results demonstrate a significant increase in energy dissipation for the antiproton beam.

In the left-hand panels of Fig. 2 the distribution of detected transverse energy per event, $E_{\rm trans} = \sum E_i \sin^2\theta_i$, is compared for the $\bar{p}$ and π^- beams. Again greater energy dissipation is indicated with the antiproton beam. However, it should be noted that while transverse energy is expected to be a first-order indicator of the excitation energy, $E_{\rm trans}$ includes contributions from preequilibrium processes that occur prior to the breakup of the thermalized system. Thus the total charged-particle multiplicities and $E_{\rm trans}$ are not ideal indicators of thermalized excitation energy.

In order to characterize the properties of the targetlike residues, it is necessary to differentiate between charged

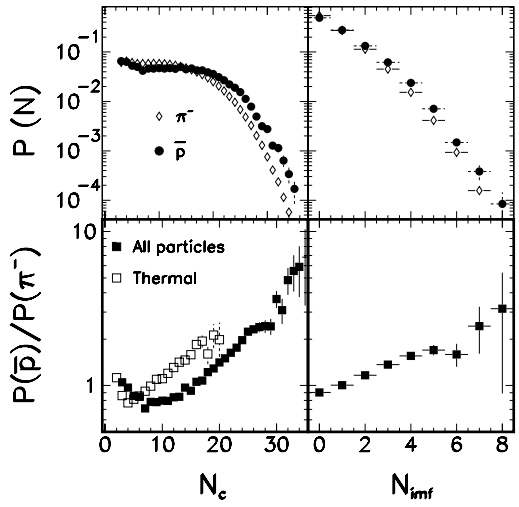

FIG. 1. Left: Measured charged-particle multiplicity distribution for $\bar{p}$ and π^- beams (top) and the ratio of the probability for a given multiplicity for each beam, $P(\bar{p})/P(\pi^-)$ (bottom). Right: Same figures for IMFs only. Note log scale on ordinate. In lower left panel open squares show $\bar{p}/\pi^-$ probability ratio for thermal charged particles.

particles associated with the fast cascade and those which originate from a thermal-like source. We define thermal-like charged particles as protons with kinetic energy $K_i^p \leq$ 30 MeV and complex particles with

$$K_i^{\rm CP} < (9.0Z_i + 40)\ \text{MeV}, \qquad (1)$$

where $K_i^{\rm CP}$ is the kinetic energy of each charged particle in an event, transformed into the source frame. This definition is based on a systematic analysis of spectral shapes as a function of total observed charge and IMF multiplicity in the 4.8 GeV ^{3}He + ^{197}Au reaction [10,14,16]. The spectra measured in E900 exhibit nearly identical

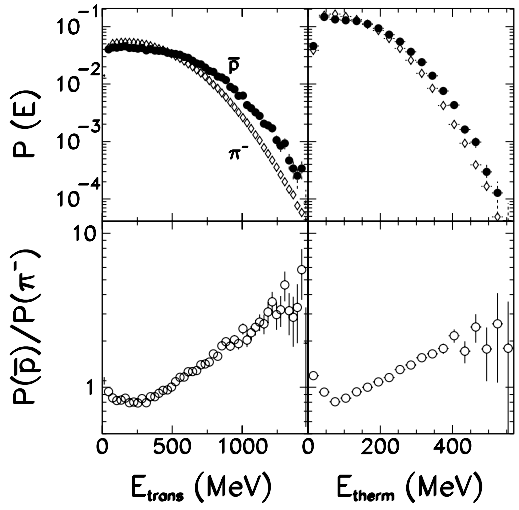

FIG. 2. Upper: Probability distribution for detected transverse (left) and thermal (right) energy deposition in the 8 GeV $\bar{p}, \pi^-$ + ^{197}Au reactions. Lower: Ratio of $\bar{p}/\pi^-$ probability as a function of transverse and thermal energy.

behaviors in the character of their evaporationlike peak and hard exponential tails. Nearly all of the IMF yield is included in the thermal gate of Eq. (1). In the right-hand panel of Fig. 2 the distribution of $E_{\rm therm}$, the energy sum of all thermal charged particles in an event, is compared for the $\bar{p}$ and π^- beams. The results, along with the corresponding probability ratios, also suggest that larger excitation energies are reached in the $\bar{p}$-induced reactions.

The $\bar{p}/\pi^-$ probability ratio for the thermal charged-particle multiplicity distributions ($N_{\rm therm}$) is shown as open squares in the lower left panel of Fig. 1. These ratios are observed to be similar to those for IMFs. The comparison of $N_{\rm th}$ and N_c in Fig. 1 reveals much larger values for total charged particles than for the thermal component. This behavior is consistent with a scenario in which only a fraction of the $\bar{p}$ annihilation energy is converted into internal excitation energy, the remainder appearing in the form of fast particles [17].

Excitation-energy distributions have been determined experimentally on an event-by-event basis according to the prescription,

$$E^* = \sum_i^{M_c} K_i^{\rm CP} + M_n\langle K_n\rangle + Q + E_\gamma\,. \qquad (2)$$

Here $K_i^{\rm CP}$ is summed over all charged particles detected in an event of multiplicity M_c, transformed event by event into the source frame. We make two assumptions with regard to the fragment kinetic energy acceptance. The first employs the thermal energy definition of Eq. (1). The second approach includes all particles up to $K_i^{\rm CP}/A \leq 30$ MeV/nucleon, according to [18]. Fragments with energies between the upper limits of Eq. (1) and Ref. [18] correspond to the hard tails of our spectra.

The second term in Eq. (2) involves the neutron multiplicity M_n and the average neutron kinetic energy $\langle K_n\rangle$. Measured charged-particle vs neutron correlations were used to determine M_n [9] and $\langle K_n\rangle$ was initially estimated from Coulomb-corrected proton spectra and then iterated to obtain a self-consistent value $\langle K_n\rangle = 3/2T_{\rm th}$, where $T_{\rm th} = (E^*/a)^{1/2}$ and $a = A/11$ MeV^{-1}. The reconstructed event serves to define the binding energy difference Q. The small amount of undetected energy from photon decay of the primary fragments is about a 2% effect, assumed to be proportional to the total event multiplicity. The experimentally deduced quantities of Eq. (2) were corrected for ISiS geometry to obtain the final value of E^*. We stress that both $\bar{p}$ and π^- data were measured and analyzed identically.

Because of the experimental trigger, the reconstruction procedure is uncertain below $E^* < 250$ MeV, where neutron emission dominates. The charge of the excited residue was obtained by subtracting the measured fast charged particles from the target charge, corrected for geometrical acceptance and folded by the corresponding angular distribution. The multiplicity of fast neutrons $M_n^{\rm fast}$ is taken to be $1.93 \times M_p^{\rm fast}$, where $M_p^{\rm fast}$ is the corrected multiplicity of fast protons ($E_p > 30$ MeV). This procedure is intermediate between the experimental systematics of Ref. [8] and the N/Z of the target [19].

In Fig. 3 the top panel shows the reconstructed distribution of excitation energy for the thermal fragment kinetic energy acceptance of Eq. (1). At the 1% probability level for our normalization (vertical lines in Fig. 3), the excitation energy per nucleon is $E^*/A = 9.0$ MeV and 10.3 MeV for the π^- and $\bar{p}$ beams, respectively. The excitation energy enhancement with antiprotons appears to grow with increasing E^*, as is apparent when the probability ratio for the two beams is examined. In the bottom frame of Fig. 3, the probability of reaching the highest excitation energies is seen to be at least 2 times greater for antiprotons than for π^- beams at the maximum deduced values, $E^* \sim 1.7$ GeV. However, these values at the 10^{-4} probability level must be interpreted with caution due to fluctuation effects. Nonetheless this suggests that $\bar{p}$ statistics comparable to those obtained with pions might produce a significant enrichment of high-E^* events, and perhaps extend the caloric curve into the vaporization regime [13].

In Table I the enhanced cross section for producing high excitation-energy residues with $\bar{p}$ beams is quantified by comparing with other hadron and light-ion data [9,14]. The comparison shows the fraction of events that exceed the multifragmentation threshold for Au-like residues ($E^* \gtrsim 800$–1000 MeV [5–7]), compared to all events with $E^* > 400$ MeV. The integrated results indicate an enhancement of up to 50% for $\bar{p}$ beams relative to π^- in this study and significantly larger enhancements relative to the 4.8 GeV ^{3}He [14] and 2.1 GeV/c $\bar{p}$ [9] studies. With respect to the LEAR results, where little evidence for multifragmentation was observed, we find that the average event with $E^* > 1000$ MeV decays via the emission of three or more $Z \geq 3$ fragments. Thus, the difference between these two experiments appears to

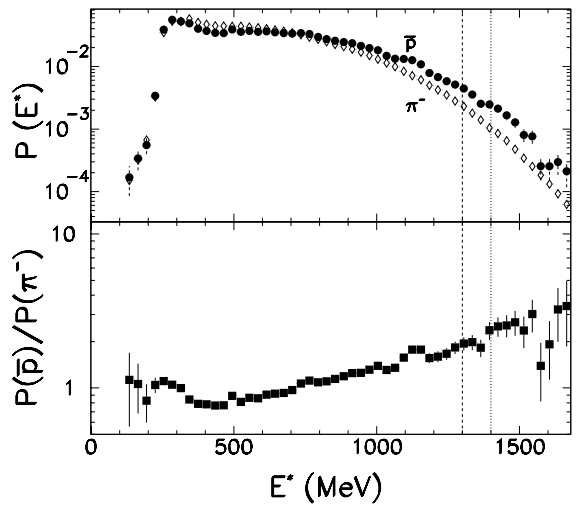

FIG. 3. Upper panel: Excitation-energy probability distributions for reactions of 8 GeV/c π^- (diamonds) and $\bar{p}$ (circles) with ^{197}Au. Lower panel: Ratio of excitation-energy probability for $\bar{p}$ relative to that for π^-. E^* values beyond the vertical lines (dashed: π^-; solid: $\bar{p}$) account for 1% of events.

TABLE I. Ratio of the integrated events beyond multifragmentation threshold to events beyond 400 MeV.

Beam	p (GeV/c)	T (GeV)	$\frac{P(E^*>800\ \text{MeV})}{P(E^*>400\ \text{MeV})}$	$\frac{P(E^*>1000\ \text{MeV})}{P(E^*>400\ \text{MeV})}$
$\bar{p}$	8.0	7.1	0.41	0.18
π^-	8.0	7.9	0.32	0.12
^{3}He [12]	7.6	4.8	0.22	0.053
$\bar{p}$ [9]	2.1	1.2	0.068	0.003

be explained by the much higher probability at 8 GeV/c for events that exceed the multifragmentation threshold.

In Fig. 4 the data are compared with predictions of the intranuclear cascade code QGSM of Toneev [3] for the excitation energy and mass distributions of heavy residues that survive the fast cascade (stopped after $\tau = 30$ fm/c). The calculation assumes random impact parameters and the default values of the code, which reproduce other cascade results at lower beam momenta ($\leq$3 GeV/c). The two left-hand frames compare the experimentally derived excitation-energy distributions for π^- (top) and $\bar{p}$ (bottom) beams. Both the thermal definitions of Eq. (1) and that of [18] are shown. Although the relative excitation-energy enhancement with $\bar{p}$ beams is qualitatively reproduced, the QGSM prediction overestimates the experimentally derived excitation energies for both projectiles. On the right, the mass distributions of the reconstructed residues are compared with the QGSM. The model predicts slightly less mass loss than deduced from the data using the thermal assumption, but is in relative accord with the more inclusive acceptance. The success in describing the residue mass while at the same time overpredicting the E^* distribution suggests that the probability for pion reabsorption may be too high in the code.

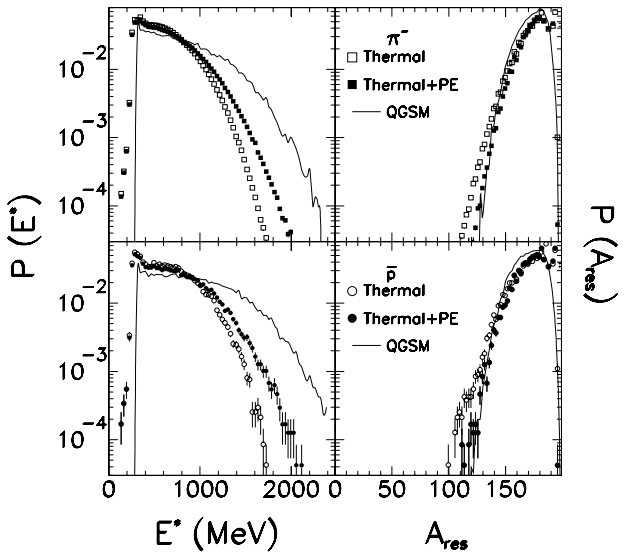

FIG. 4. Left: Distribution of excitation energy in targetlike residues for π^- (upper) and $\bar{p}$ (lower) beams. Open circles denote thermal particles only, solid circles include all energies up to $E/A \leq 30$ MeV and lines give INC prediction [4]. Right: Residue mass distributions; all symbols are the same as for left-hand panels.

In summary, we have compared energy deposition in heavy residues formed in reactions induced by 8 GeV/c π^- and antiproton beams. Experimental signals such as the raw multiplicity distributions, thermal and transverse energy distributions, extend to significantly higher values for antiproton beams relative to other hadron projectiles. Event reconstruction of the residue mass and excitation-energy distributions confirm that the probability for reaching the highest excitation energies is significantly enhanced in antiproton-induced reactions at this beam momentum. An increase in cross section of nearly 50% is observed for $E^* > 1000$ MeV and multifragmentation is the predominant decay mode for these events. The experiment suggests that 5–10 GeV/c antiprotons provide the most effective beams for investigation of the thermal aspects of multifragmentation.

The authors thank J. Vanderwerp, W. Lozowski, K. Komisarcik, and R. N. Yoder at IUCF and P. Pile, J. Scaduto, L. Toler, J. Bunce, J. Gould, R. Hackenberg, and C. Woody at AGS for their assistance with these experiments. This work was supported by the U.S. Department of Energy and National Science Foundation, the National Sciences and Engineering Research Council of Canada, the Polish State Committee for scientific research, and the Robert A. Welch Foundation.

*Present address: Los Alamos National Laboratory, Los Alamos, NM 87545.

[1] D. Strottman and W. R. Gibbs, Phys. Lett. **149B**, 288 (1984).
[2] J. Cugnon *et al.*, Nucl. Phys. **A470**, 558 (1987); Phys. At. Nucl. **57**, 1075 (1994).
[3] V. Toneev, N. S. Amelin, K. K. Gudima, and S. Yu. Sivoklokov, Nucl. Phys. **A519**, 463 (1990).
[4] G. Wang, K. Kwiatkowski, V. E. Viola, W. Bauer, and P. Danielewicz, Phys. Rev. C **53**, 1811 (1996).
[5] W. A. Friedman, Phys. Rev. C **42**, 667 (1990).
[6] J. Bondorf *et al.*, Nucl. Phys. **A443**, 221 (1985).
[7] D. H. E. Gross, Rep. Prog. Phys. **53**, 605 (1990).
[8] D. Polster *et al.*, Phys. Rev. C **51**, 1167 (1995).
[9] F. Goldenbaum *et al.*, Phys. Rev. Lett. **77**, 1230 (1996); L. Pienkowski *et al.*, Phys. Lett. B **336**, 147 (1994).
[10] K. B. Morley *et al.*, Phys. Rev. C **54**, 737 (1996).
[11] W.-c. Hsi *et al.*, Phys. Rev. Lett. **79**, 817 (1997).
[12] L. Beaulieu *et al.*, Phys. Lett. B **463**, 159 (1999).
[13] J. Pochodzalla *et al.*, Phys. Rev. Lett. **75**, 1040 (1995).
[14] K. Kwiatkowski *et al.*, Phys. Lett. B **423**, 21 (1998).
[15] K. Kwiatkowski *et al.*, Nucl. Instrum. Methods Phys. Res., Sect. A **360**, 571 (1995).
[16] D. S. Bracken, Ph.D. thesis, Indiana University, 1996.
[17] P. McGaughey *et al.*, Phys. Lett. B **266**, 264 (1986).
[18] J. A. Hauger *et al.*, Phys. Rev. Lett. **77**, 235 (1996).
[19] I. A. Pshenichnov *et al.*, Phys. Rev. C **52**, 947 (1995).